Available online at www.sciencedirect.com
SCIENCE DIRECT
Journal of Power Sources 146 (2005) 51–57
JOURNAL OF POWER SOURCES
www.elsevier.com/locate/jpowsour

Some studies on electrolytes for lithium ion batteries

Zhaoxiang Wang *, Yongsheng Hu, Liquan Chen

Laboratory for Solid State Ionics, Institute of Physics, Chinese Academy of Sciences, Beijing 100080, China

Abstract

The recent progress of investigation in this laboratory on some interesting electrolytes for lithium ion batteries is summarized. Nano-Al_2O_3 filler was found to act as a solid solvent in the $LiClO_4$/polyacrylonitrile electrolyte system. Novel room temperature molten salt was prepared and showed a series of interesting electrochemical properties. Addition of vinyl ethylene carbonate (VEC) into propylene carbonate based electrolyte helped to form a compact solid electrolyte interphase layer on graphite anode during the first discharge process.

Keywords: Electrolytes; Lithium ion batteries; Electrochemical properties

1. Introduction

The electrolyte for lithium ion batteries can be roughly classified into solid and liquid electrolytes and (room temperature) molten salt. Polymer electrolyte is currently the most popular solid electrolyte for lithium ion batteries due to its good mechanical and electrochemical properties. Introduction of nanoscale inorganic fillers such as Al_2O_3, TiO_2 and SiO_2 has been proved effective in enhancing the mechanical strength and conductivity of the polymer electrolyte [1,2]. However, there are still debates and even contradicted reports as to why adding nanosized ceramic particles can improve the ionic conductivity of the polymer electrolytes [3,4].

Nanoscale ceramic additives have two important common features: large specific surface areas and grains covered with various Lewis acidic or basic groups. The interactions between these surface groups and the ionic species of the salt are responsible for the observed conductivity enhancement [3]. Nevertheless, direct experimental evidence is rare of the influence of the ceramic filler on these interactions. As the fillers affect the physical and electrochemical performances of the composite polymer electrolyte via their surface groups, the contents of the additives in this work are much higher than in practical composite polymer electrolytes (usually about 10–20 wt.%) so as to increase the total contact area between the filler particles and the polymer electrolyte and "magnify" these interactions.

Propylene carbonate (PC) based electrolytes have been attractive to the scientists due to its low melting point, high dielectric constant and high flash point. However, the severe co-intercalation of PC molecules and the solvated Li^+ ions into graphitic electrode prevents its practical application in lithium ion batteries. Efforts to improve the compatibility of the PC-based electrolytes with the graphitic electrode include modification to the graphite surface [5] and introduction of some functional additives, especially vinylene carbonate (VC) [6]. Indeed, VC-added PC-based electrolyte is very effective in forming a passivating layer prior to the intercalation of Li^+ ions into graphitic electrode. However, an intrinsic drawback of VC is that it tends to get polymerized. In this report, vinyl ethylene carbonate (VEC) replaces VC as a film-forming additive because the former is supposed to be more stable due to its electron-rich double bond.

In recent years, some room temperature molten salts have been reported as a novel type of liquid electrolytes for lithium ion batteries. These electrolytes usually have a low melting point and are stable until very high temperature, in comparison to the traditional liquid electrolytes. This type of electrolytes is special because they are composed exclusively of cations and anions, different from the ordinary liquid electrolytes. We previously reported that lithium bis(trifluoromethane sulfone)imide (LiTFSI)/urea complex

* Corresponding author.

0378-7753/$ – see front matter © 2005 Published by Elsevier B.V.
doi:10.1016/j.jpowsour.2005.03.092

system was a room temperature molten salt (RTMS) with eutectic temperature of −37.7 °C [7]. However, the performance of the LiTFSI/urea complex is not satisfactory. Here we will replace urea with acetamide because of the dipolar nature of the latter.

2. Experimental

Polyacrylonitrile (PAN, $M_w = 20{,}000$) and/or anhydrous $LiClO_4$ were first dissolved in a suitable amount of propylene carbonate (PC) and then dry commercial Al_2O_3 (with particle size of about 30 nm) was added to the solution. The mixture was heated and mechanically stirred at 120 °C until most of the solvent was evaporated in air in about 2 h. The solvent-free composite material was mixed with dry KBr and pressed into pellets in an Ar-filled glove box ($H_2O < 1$ ppm). The pellets were stored in a vacuum oven (120 °C, 0.1 bar) for more than 7 days. Specific infrared spectroscopic check indicated that the solvent residual is not detectable and its interference to the IR spectrum is negligible.

PC (battery grade), VEC (99%, Aldrich) and LiBETI (99%, 3 M Inc.) were mixed for 1 M LiBETI/PC and 1 M LiBRTI/PC/VEC electrolytes in the glove box. Graphite/Li test cells were assembled in the glove box with Celgard 2300 as the separator and Cu foil as the current collector for the graphite electrode.

LiTFSI (99.9%, 3 M Inc.) was dried in vacuum at 140 °C for a week. Acetamide (99%, Alfa) was dried with P_2O_5 in vacuum at 55 °C for a week. RTMS was prepared by simply mixing LiTFSI and acetamide in the glove box. Homogeneous liquids with molar ratios of LiTFSI and acetamide between 1:2 and 1:6 were obtained directly by stirring the mixtures at room temperature and then stored overnight. The samples were sealed in disposable optical glass test tubes for the Raman measurements.

Bruker RFS 100 Fourier transformed Raman spectrometer was used for the Raman scattering. The scattered light was collected in the direction of 180° to the incident light (backscattering geometry). The solid sample was mixed with dry KBr and pressed into pellet while a droplet of the liquid sample was spread on a dry KBr pellet. All samples were kept in sealed bottles filled with Argon before they were transferred into the vacuum chamber of BIO-RAD FTS-60 FTIR spectrometer. The resolution of the Raman and IR spectrometers was set to 2 cm^{-1}.

3. Results and discussion

3.1. Solid solvent effects of ceramic nano-Al_2O_3 filler in polymer electrolyte

Solid $LiClO_4$ has multiple bands at around 1120 cm^{-1} ($\nu_3(F_2)$), a single band at 966 cm^{-1} ($\nu_1(A_1)$), and bands at 466 and 486 cm^{-1} ($\nu_2(E)$) in the IR spectrum. Its characteristic $\nu_4(F_2)$ mode is particularly sensitive to the local anionic

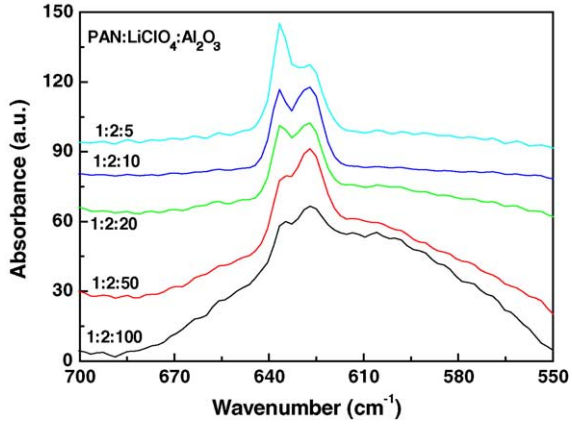

Fig. 1. Spectral evolution of the components of the $\nu_4(F_2)$ mode of ClO_4^- with increase of Al_2O_3 content in nano-composite polymer electrolyte PAN/$LiClO_4$/Al_2O_3.

environment. Strong bands at 627 and 636 cm^{-1} are observed in $LiClO_4/Al_2O_3$ with a weight ratio of 1:1. The band at 636 cm^{-1} is attributed to the contact ion pairs while the line at 627 cm^{-1} is assigned to the free anions that do not interact directly with Li^+ cation [8]. Fig. 1 shows the ceramic content dependence of the relative intensity of the 634 and 627 cm^{-1} bands. In samples with high Al_2O_3 contents, the 634 cm^{-1} band is very weak and the 627 cm^{-1} band becomes the dominant. This indicates that the ionic association of the ClO_4^- anions becomes less obvious and most of the ClO_4^- anions become free with the increasing ceramic content. This demonstrates that addition of ceramic Al_2O_3 helps to dissociate the Li^+-ClO_4^- association in solid salt. In this respect, the nanosized ceramic filler acts as a solid solvent to the salt in the composite.

Strong interaction between the nitrile of PAN and the Li^+ ions has long been observed in this laboratory [9]. The C≡N stretching band is located at 2240 cm^{-1} in pure PAN. A new component is observed at 2270 cm^{-1} when C≡N···Li^+ interaction occurs. Fig. 2a shows the influence of the content of nanoscale ceramic additive on the polymer-salt interaction. Clearly, strong C≡N···Li^+ interactions take place when the content of the salt is high (Fig. 2b) and/or the content of the additive is low. As the content of the ceramic increases, the C≡N···Li^+ interaction becomes less obvious and even undetectable. These results indicate that the addition of ceramic powder weakens the interaction between the nitrile group and the Li^+ ions in the electrolyte. Meanwhile, the introduction of ceramic powder weakens the association between the cations and the anions and makes the content of free anions increase.

The above observation can be attributed to the possible competition between the ceramic particle and the Li^+ cations on the association with the nitrile group of PAN as evidenced in Fig. 3. Only a single band is observed at 2240 cm^{-1} in pure PAN. With the increase of the ceramic content in the PAN/Al_2O_3 composite, a weak but obvious shoulder appears at 2254 cm^{-1} in the spectrum. Its intensity increases with increasing Al_2O_3 content in the composite. Such spectral

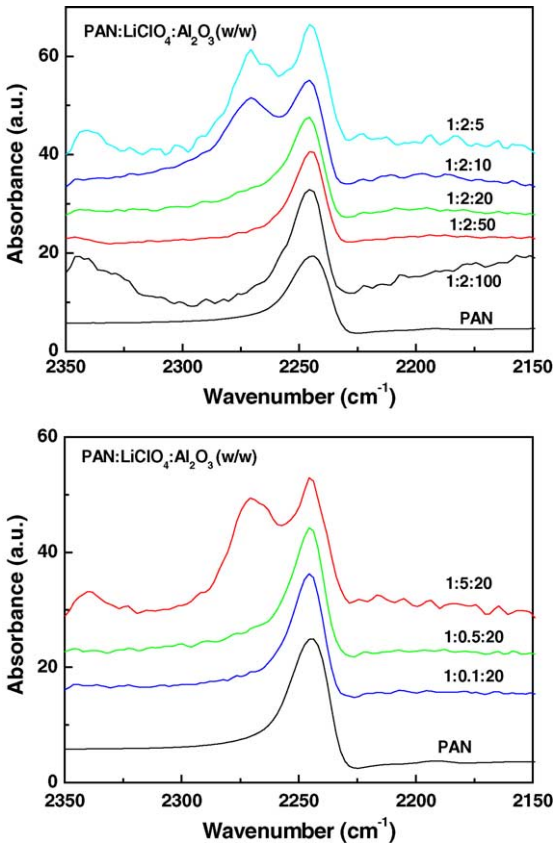

Fig. 2. Dissociation effect of Al_2O_3 on the Li···N≡C–R complex in PAN/$LiClO_4$/Al_2O_3 depending on the contents of (a) Al_2O_3 and (b) $LiClO_4$.

variation should be attributed to the interaction between the surface groups on the nanoparticle and the polymer. It is also worth pointing out that such a phenomenon is not observed in composites containing $LiClO_4$, probably due to the stronger competition of the Li^+ ion than the H^+ ions.

Similar spectral features have been observed in PAN/$LiClO_4$ with various contents of MgO, SiO_2 and TiO_2 in this laboratory. The similarity of spectral features in the composites with different ceramic oxides implies that the

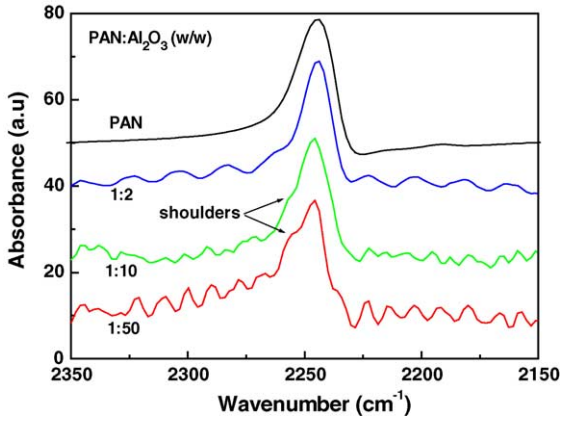

Fig. 3. Association between the surface group of Lewis acidic Al_2O_3 and the nitrile group of PAN (Al_2O_3–OH^+···N≡C–R).

surface properties of the ceramic filler are more important that the composition of the filler itself on interacting with the components of the polymer electrolytes. In the case of nano-composite polymer electrolyte incorporating Al_2O_3 grains, the dependence of the conductivity enhancement on the nature of the filler surface group may be satisfactorily explained in terms of the Lewis acid–base type interactions involving different types of surface groups [1,10]. Based on these ideas, Jayathilaka et al. [3] attributed the enhanced conductivity of $(PEO)_9$/LiTFSI/Al_2O_3 system to the newly created pathways due to Lewis acid–base interaction between surface groups on the nano-ceramic filler and ions of the salt. However, they ignored the effects of the ceramic filler on the interaction between the charge carriers and the polymer and on the ionic association in such a model. Our experimental facts demonstrate, nevertheless, that these effects have to be considered.

The electrochemical, mechanical and electrolyte-electrode interfacial performances of the PAN-based nanocomposite electrolytes are very similar to that of PEO-based electrolytes. Many authors employed the mechanism for PEO-based composite electrolytes (usually solvent-free) described above to explain the enhanced conductivity in PAN-based electrolytes [4]. Our early reports [11] based on ^7Li NMR results have shown that there are three possible states for the Li^+ ions in plasticized polymer (gel) electrolytes: fast-moving ions in the gel (liquid-like) state, slow-moving ions in solid PAN and the chemical shifts due to ions associated with the plasticizer (solvent). Obviously free Li^+ ions moving in the gel contribute the most to the conductivity of the polymer electrolyte. In a practical polymer electrolyte, the slow moving ions like the contact ion pairs, ionic clusters involved or uninvolved with the nitrile groups of PAN should be avoided. This is different from that in the PEO-based polymer electrolyte where Li^+–O association is promoted because the segmental movement of the ethylene oxide makes the most important contribution to the ionic conductivity. Keep this in mind, the interaction mechanism proposed by Jayathilaka et al. [3] and Croce et al. [10] cannot explain the enhanced ionic conductivity of PAN-based polymer electrolytes with nanoscale ceramic oxides. Based on the above FTIR studies on the spectral changes induced by the addition of nanoscale Al_2O_3, another possible explanation is proposed to interpret the effects of the nanoscale ceramic oxides on the ionic conductivity and ionic transference number, also based on the Lewis acid–base interactions.

In a PAN-based electrolyte with or without plasticizer (solvent), severe associations (R–C≡N···Li^+ associates and $Li^+ClO_4^-$ contact ion pairs) take place when the content of the lithium salt ($LiClO_4$, for example) is high. When acidic nanoscale ceramic Al_2O_3 is added, the strong polarable nature of the ClO_4^- anion will dissociate the $Li^+ClO_4^-$ ion pairs and make the Li^+ ions free (Fig. 4a). Meanwhile, the nitrile-associated Li^+ ions also become free due to the stronger polarable ability of the H^+ on the acidic group than

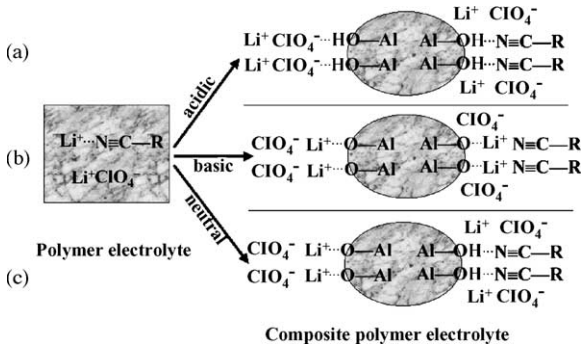

Fig. 4. Schematic demonstration of the dissociation effects of Lewis acidic (a), basic (b) and neutral (c) surface groups on nano-Al_2O_3 particles.

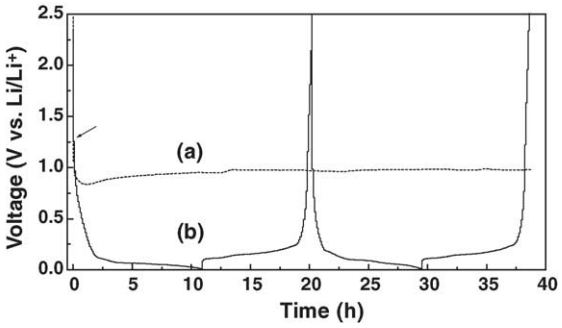

Fig. 5. Voltage profiles of the first two cycles of graphite/Li cells with (a) 1 M LiBETI/PC and (b) 1 M LiBETI/PC/VEC (95:5 by volume) as electrolytes between 2.5 and 0.01 V vs. Li/Li^+ at 0.156 mA cm^{-2}.

the Li^+ ions towards the nitrile group of PAN. Such interactions will increase the content of free Li^+ ions in the composite electrolyte and enhance the ionic conductivity. This suggestion is supported with the increased intensity ratio, I_{627}/I_{634}, and the disappearance of the characteristic line at 2270 cm^{-1} with the increase of Al_2O_3 content in the composite polymer electrolyte as shown in Fig. 3. In addition, the Li^+ cation transference number in such a composite is expected to be higher than with other types of surface groups because the anions are trapped by the oxygen atoms on the surface of the nanoparticles.

For Al_2O_3 with Lewis basic surface groups, the polar O atoms on its surface will interact with the Li^+ ions and dissociate the $Li^+ClO_4^-$ ion pairs (Fig. 4b). On the other hand, the strong interaction between O and Li^+ ions will dissociate the R–C≡N···Li^+ bonding and free the ClO_4^- anions. During their migration under an applied potential, the polar Li^+ ions dissociated from the salt can interact with these polar oxygen atoms via transient hydrogen bonding. The cations can keep H-bonded to the oxygen only temporarily. Therefore, there will be extra charge carriers to migrate in the vicinity of the filler grains. As the content of the ceramic oxide is rather high (10–20 wt.% in a practical composite polymer electrolyte), these intermittent co-ordinations can still provide a pseudo-continuous effective pathway for the transport of the charge carriers. The interaction of the basic surface groups with Li^+ or positively charged triplets leads to the limitation of the salt-polymer interaction. For the other two groups of electrolytes studied, the effect of the competition of acidic or neutral surface groups of the filler with Li^+ ions in the complexation of the polyether oxygen is observed.

As for the neutral Al_2O_3 additives, both interactions described above can exist and more concentrated charge carriers be expected (Fig. 4c). However, as the anions can re-associate with the Li^+ cations and form new associates, the actual concentration of the charge carriers will be lower than in the above two cases.

As no experimental evidence is obtained in this work concerning any structural variation of the C–C chain of the polymer, the involvement of the polymer chain in ionic transport is rather unaffected due to the addition of the filler in agreement with the previous reports. However, cation migration and the number of ion pairs will definitely be affected by the presence of these acidic fillers, in contrast with the model of Jayathilaka et al. [3].

3.2. VEC as SEI-forming additive of graphite/Li cells with PC-based electrolytes

Fig. 5 shows the voltage profiles of graphite/Li cells in the first two cycles with and without the addition of VEC into LiBETI/PC electrolytes. For the cell without an additive, only a long discharge plateau at ca. 0.9 V was observed due to the co-intercalation of PC and the solvated Li^+ ions into graphite (Fig. 5a). The electrode potential cannot reach the potential of Li^+ intercalation (<0.25 V versus Li/Li^+) before the electrode is damaged completely. In contrast, the long discharge plateau at ca. 0.9 V disappears and profile becomes quite similar to that of graphite in, for example, commercial 1 M $LiFP_4$/EC/DMC electrolyte after 5% (v/v) of VEC is added into LiBETI/PC electrolyte. The voltage drops rapidly at first and then slowly between 1.3 and 0.2 V, corresponding to the electrolyte decomposition on graphite. Below 0.2 V, the Li^+ ions are intercalated into graphite. This results in the formation of a passivating film on the graphite surface. The coulombic efficiencies of the first, second and 30th cycles are 85, 98 and 97.8%, respectively, suggesting that the film on the graphite surface is effective and stable.

Further study to the graphite electrode discharged to 0.01 V by FTIR (Fig. 6) indicates that $ROCO_2Li$ (2853–2957 cm^{-1} bands for CH stretching, 1667 cm^{-1} band for C=O asymmetric stretching, 1338 cm^{-1} band for symmetric C=O stretching, and the 832 cm^{-1} band for OCO_2 deformation), Li_2CO_3 (1435–1492 cm^{-1} band for CO_3^{2-} stretching, and the 870 cm^{-1} band for CO_3^{2-} deformation), and ROLi (1187 and 1087 cm^{-1} bands for C–O stretching and the 508 cm^{-1} band for Li–O vibration) are the main components of the passivating film on graphite particles. These are actually the typical components of the SEI layer on most anodes for lithium (ion) batteries.

An interesting phenomenon is observed when 1 M LiBETI/PC/VEC (95:5 by volume) is used in lithium cells

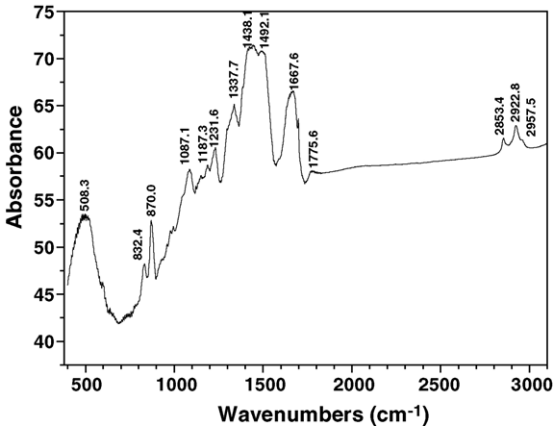

Fig. 6. FTIR spectrum of the graphite electrode discharged to 0.01 V in 1 M LiBETI/PC/VEC electrolyte.

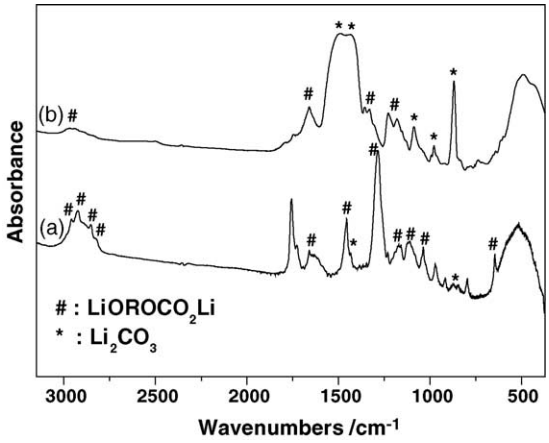

Fig. 8. FTIR spectra of MCMB electrodes discharged to 0.01 V in 1 M LiBETI/PC/VEC electrolyte.

with different graphitic electrode. Although the cycling performances of flake graphite (SLP30) does not change much at low and high current densities, the cycling performances of mesocarbon microbeads (MCMB, Shanshan®, China) are significantly different at low and high current densities. At a low current density (0.094 mA cm^{-2}), MCMB shows three discharge plateaus at 1.25 V (20 mAh g^{-1}), 0.8 V (868 mAh g^{-1}) and below 0.25 V (298 mAh g^{-1}) (Fig. 7). The discharge plateaus at 1.25 and below 0.25 V correspond to the decomposition of VEC and the intercalation of Li^+ ions into the graphite, respectively. This means that the electrolyte decomposition does not form an effective SEI layer to prevent the co-intercalation into MCMB.

The irreversible capacities of MCMB in the first cycle decreases to 39 mAh g^{-1} when the current density is increased to 0.25 mA cm^{-2}, corresponding to coulombic efficiencies of 88.8%. The discharge plateau at ca. 0.8 V disappears.

Ota et al. [12] proposed that the solvent molecules undergo one- and two-electron reduction processes at the low and high charge/discharge current densities respectively. Based on this proposal, density functional theory (DFT) calculation was carried out. It shows that the decomposition products of VEC are $LiOCH(CH{=}CH_2)CH_2OCOCH(CH{=}CH_2)$–$CH_2OCO_2Li$ and Li_2CO_3 undergoing one- and two-electron reduction processes, respectively. This is confirmed by FTIR spectra (Fig. 8). The pronounced bands around 2820 to 2960 cm^{-1} (ν CH), 1655 cm^{-1}(ν_{as} C=O), 1455 cm^{-1} (δ CH/CH_3), 1286 cm^{-1} (ν_s C=O), 1037 to 1170 cm^{-1} (ν C–O), 916 cm^{-1} (δ CH_2) and 645 cm^{-1} (δ OCO_2) are typical of lithium alkylcarbonates ($LiOROCO_2Li$) [13]. The band at 1776 cm^{-1} might be related to polycarbonate that is formed by some polymerization of VEC. The bands around 1437 and 1501 cm^{-1} (ν CO_3^{2-}), 1090 cm^{-1} (ν C-O) and 870 cm^{-1} (δ CO_3^{2-}) are characteristic of Li_2CO_3 [13]. Compared with the two FTIR spectra, it can be seen clearly that the main reductive products of VEC at the low current density is $LiOROCO_2Li$ whereas Li_2CO_3 is the main product at high current density.

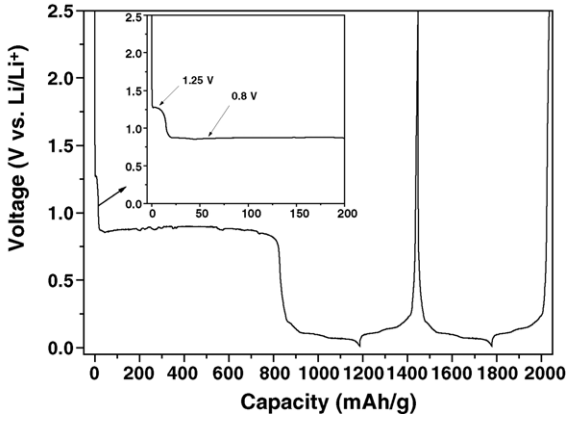

Fig. 7. Voltage profiles of MCMB electrodes in1 M LiBETI/PC/VEC in the first two cycles at 0.094 mA cm^{-2} (the inset is its selected part around 1.0 V).

3.3. Characterization of a room temperature molten salt $LiTFSI/CH_3CONH_2$

The melting points of LiTFSI and acetamide are 234 and 81.2 °C, respectively. Mechanical mixing LiTFSI and acetamide with molar ratio between 1:2 and 1:6 and stirring the mixture for overnight lead to the formation of a homogeneous liquid at room temperature.

The ionic conductivity of the RTMS electrolyte with several compositions as a function of temperature is shown in Fig. 9. The conductivity temperature relationship fits well to the VTF equation (Fig. 9b)

$$\sigma(T) = AT^{-1/2} \exp\left[\frac{-E_a}{R(T - T_0)}\right]$$

indicating that the ion transport is dominated by the mobility of the solvent molecule and the conductivity depend on the free volume of the solvent in these RTMSs. The ionic conductivity of the RTMS electrolyte at molar ratio of 1:4

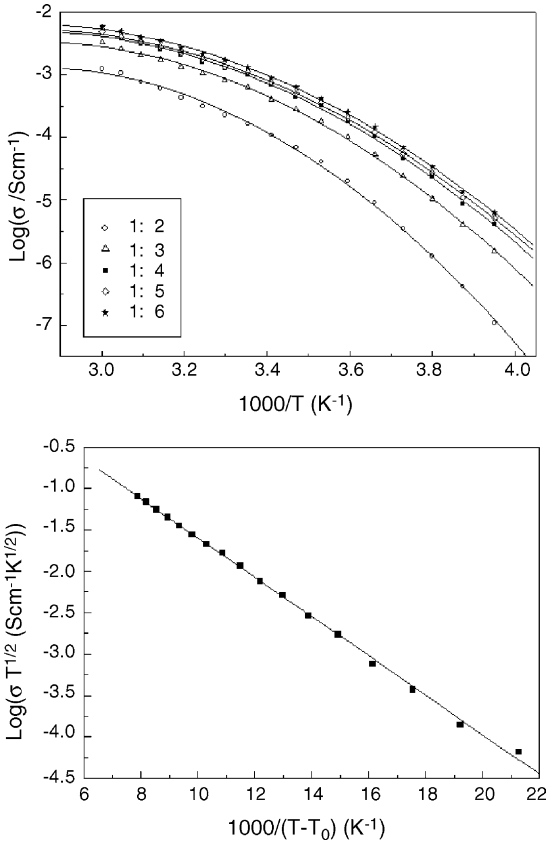

Fig. 9. The Arrhenius plot of the RTMS with various molar ratios and the VTF plot of the RTMS at a molar ratio of 1:4.

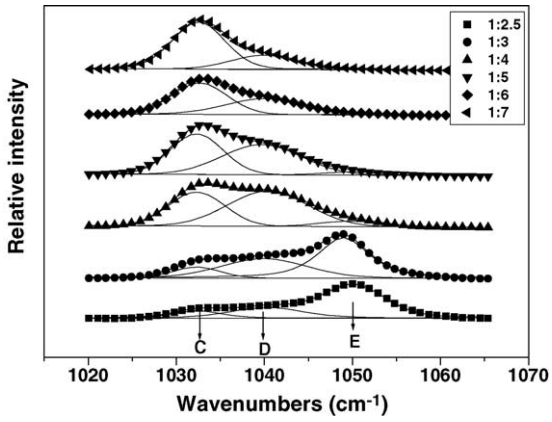

Fig. 10. Raman spectra of the SO_3 symmetric stretching band in the $LiCF_3SO_3$/acetamide composite with different molar ratios. The three lower solid Lorentzian lines in each spectrum correspond to the fitted results, whereas the upper solid line represents the sum of these three fitted bands.

reaches 1.07×10^{-3} S cm^{-1} at room temperature and rises to 4.41×10^{-3} S cm^{-1} at 60 °C. The nominal activation energies (E_a) were calculated and found to increase with the increasing salt concentration in the complex.

Electrochemical stability window of the RTMS electrolyte with molar ratio of 1:4 is determined by cyclic voltammetry (CV) at 25 °C at a scan rate of 0.5 mV s^{-1}. In an electrochemical cell, copper and nickel foils are used as working electrode separately. Li foils are used as the reference and counter electrodes. The CV shows that the RTMS is reduced at 0.7 V on copper and oxidized on nickel at 4.4 V versus Li/Li$^+$.

Raman spectroscopy is applied to probe interaction between the salt and acetamide and between the cation and anions in the RTMS. Fig. 10 shows the Raman spectra of the composite with various molar ratios in the ν_s SO_3 spectra region. It contains multiple components due to the coexistence of different ionic species. PEAKFIT software is used to fit this band. The three fitted Lorentzian components are located at 1032, 1040 and 1050 cm^{-1}, corresponding to the "free" anions, contact ion pairs and aggregates, respectively [14]. It is not possible to distinguish between fully dissociated ions and solvent separated ion pairs since the frequency shift for the latter is expected to be small. However, the "free" anions prefer to be solvent separated ion pairs due to the strong anion–solvent interactions in the composite. The shape of the multi-component band of the ν_s SO_3 mode reveals that there are strong cation–anion interactions in the complex system over a wide range of salt concentration. The content of aggregates decreases abruptly when the salt concentration decreases from 65% at $LiCF_3SO_3$:acetamide = 1:2.5 to 8% at 1:4. Then it falls slightly when the salt concentration is further decreased. However, the relative amount of contact ion pairs initially increases with decreasing salt concentration from ca. 24% at $LiCF_3SO_3$: acetamide = 1:2.5 to 55% at 1:4. Finally it turns to decrease with decreasing salt concentration. This suggests that cation–anion interaction is enhanced with increasing salt concentration.

Cation–solvent interactions are observed on the C=O stretching mode of acetamide at 1678 cm^{-1}. The C=O stretching band changes significantly and splits into two components located at 1611 and 1668 cm^{-1} upon introducing $LiCF_3SO_3$ into the acetamide. The band at 1678 cm^{-1} is broadened and red-shifts to 1668 cm^{-1}. As there is no other observable FT-IR band in this region, the split band must originate from the strong interaction between the Li$^+$ ions and acetamide. Considering the resonance structure of acetamide, the Li$^+$ ions have a tendency to coordinate with the O atoms in the C=O group because these O atoms are negatively charged in the present complex system. This interaction results in the red-shifting of the C=O stretching mode which shifts from 1678 to 1668 cm^{-1}. The relative intensity of the component at 1611 cm^{-1} increases markedly with increasing acetamide concentration, indicating that there is a large amount of O atoms in acetamide interacting with the Li$^+$ ions and, therefore, a stronger cation–solvent interaction occurs when the acetamide concentration is high. Anion–solvent interactions are also observed on the N–H stretching mode at ca. 3200 cm^{-1} of NH_2 group by hydrogen bonding. These interactions explain why two solids can become one homogeneous liquid at room temperature.

4. Conclusions

1. Nanocomposite electrolytes PAN/$LiClO_4$/Al_2O_3 have been prepared. Infrared spectroscopic study shows that the addition of the nano-ceramics can help the dissolution of the lithium salt and the dissociation of the Li^+-nitrile. Based on the Lewis acid–base type of interactions, it is proposed that the competitions between the Li^+ ion and the hydrogen on the surface of acidic nano-oxides and between ClO_4^- anions and the oxygen on the surface of basic nano-oxides help to separate the $Li^+ClO_4^-$ ion pairs. Meanwhile, such competition also dissociates the Li^+-nitrile interactions. These interactions increase the contents of free charge carriers in the electrolytes and enhance the ionic conductivity of the nanocomposite polymer electrolytes.
2. Addition of VEC prevent the co-intercalation of solvent and the solvated Li+ ions into graphitic electrode. FTIR investigation to the discharged graphite demonstrates the formation of typical components for solid interphase layer on graphite, including $LiORCO_2ROCO_2Li$, Li_2CO_3, $LiROCO_2Li$, $(ROCO_2Li)_2$, etc. (R = alkyl group), in agreement with the DFT calculation results. Further it is found that reduction products of VEC at high and low discharge current densities on MCMB are different. High current density is beneficial because Li_2CO_3 is formed on the electrode then.
3. A novel RTMS electrolyte is obtained by mixing suitable amounts of LiTFSI and acetamide at room temperature. These room temperature molten salts show a series of good properties for potential application in Li ion batteries. The ionic conduction behavior of this RTMS electrolyte agrees well with the VTF equation because of the strong interaction between LiTFSI and acetamide. The ionic conductivity of the RTMS at molar ratio of 1:4 is 1.07×10^{-3} S cm^{-1} at 25 °C and reaches 4.41×10^{-3} S cm^{-1} at 60 °C. The formation of RTMS is attributed to the strong coulombic interactions between the cation and anion, the association between the cation and the solvent and the hydrogen bonding between the anion and the solvent.

Acknowledgments

This work was financially supported by the National Science Foundation of China (NSFC) (Contract No.50272080) and the Special Funds for Major State Basic Research Project of China (Contract No.2002CB211802).

References

[1] F. Croce, G.B. Appetcchi, L. Persi, B. Scrosati, Nature 394 (1998) 456.
[2] B. Scrosati, F. Croce, L. Persi, J. Electrochem. Soc. 147 (2000) 1718.
[3] P.A.R.D. Jayathilaka, M.A.K.L. Dissanayake, I. Albinsson, B.E. Mellander, Electrochim. Acta 47 (2002) 3257.
[4] Y.W. Chen-Yang, H.C. Chen, F.J. Lin, C.C. Chen, Solid-State Ionics 150 (2002) 327.
[5] X.D.Wu, Z.X. Wang, X.J. Huang, L.Q. Chen, Surf. Coat. Technol., in press.
[6] D. Aurbach, K. Gamolsky, B. Markovsky, Y. Gofer, M. Schmidt, U. Heider, Electrichim. Acta 47 (2002) 1423.
[7] H.Y. Liang, H. Li, Z.X. Wang, F. Wu, L.Q. Chen, X.J. Huang, J. Phys. Chem. B 105 (2001) 9966.
[8] E. Quartarone, P. Mustarelli, A. Magistris, Solid-State Ionics 110 (1998) 1.
[9] Z.X. Wang, B.Y. Huang, H. Huang, L.Q. Chen, R.J. Xue, F.S. Wang, Electrochim. Acta 41 (1996) 1443.
[10] F. Croce, L. Persi, B. Scrosati, F. Serraino-Fiory, E. Plichta, M.A. Hendrickson, Electrochim. Acta 46 (2001) 2457.
[11] Z.X. Wang, B.Y. Huang, R.J. Xue, X.J. Huang, L.Q. Chen, Solid-State Ionics 121 (1999) 141.
[12] H. Ota, T. Sato, H. Suzuki, T. Usami, J. Power Sources 97–98 (2001) 107.
[13] D. Aurbach, b. Markovsky, M.D. Levi, E. Levi, A. Schechter, M. Moshkovich, Y. Cohen, J. Power Sources 81–82 (1999) 95.
[14] R. Frech, S. Chintapalli, P.G. Bruce, C.A. Vincent, Chem. Commun. (1997) 157.